

# Flow of a spherical capsule in a pore with circular or square cross-section

X.-Q. Hu, A.-V. Salsac and D. Barthès-Biesel<sup>†</sup>

Laboratoire Biomécanique et Bioingénierie (UMR CNRS 6600),  
Université de Technologie de Compiègne, BP 20529, 60205 Compiègne, France

(Received 3 May 2011; revised 29 July 2011; accepted 17 October 2011)

The motion and deformation of a spherical elastic capsule freely flowing in a pore of comparable dimension is studied. The thin capsule membrane has a neo-Hookean shear softening constitutive law. The three-dimensional fluid–structure interactions are modelled by coupling a boundary integral method (for the internal and external fluid motion) with a finite element method (for the membrane deformation). In a cylindrical tube with a circular cross-section, the confinement effect of the channel walls leads to compression of the capsule in the hoop direction. The membrane then tends to buckle and to fold as observed experimentally. The capsule deformation is three-dimensional but can be fairly well approximated by an axisymmetric model that ignores the folds. In a microfluidic pore with a square cross-section, the capsule deformation is fully three-dimensional. For the same size ratio and flow rate, a capsule is more deformed in a circular than in a square cross-section pore. We provide new graphs of the deformation parameters and capsule velocity as a function of flow strength and size ratio in a square section pore. We show how these graphs can be used to analyse experimental data on the deformation of artificial capsules in such channels.

**Key words:** biological fluid dynamics, boundary integral methods, capsule/cell dynamics

---

## 1. Introduction

Suspensions of microparticles are common in nature and industry. The particles may be passive with a motion and deformation governed by hydrodynamic forces or they may be self-propelled like bacteria or squirmers (Pedley & Kessler 1992; Pedley 2010). In both cases, the motion of the particle depends strongly on the interfacial mechanics and kinematics.

In the present paper, we consider a special class of passive deformable particles, capsules, that consist of a liquid drop enclosed by a deformable membrane. Capsules are common in nature (red blood cells, phospholipid vesicles) and in different applications, such as pharmacology (Cole, Cad & Benameur 2008), cosmetics (Miyazawa *et al.* 2000), the food industry (Gibbs *et al.* 1999) and biomedical engineering (Rabanel *et al.* 2009). A fine control of the membrane properties is necessary to control the capsule deformation or possible breakup (to be induced or prevented depending on the application). However, measuring the mechanical properties of the capsule membrane is difficult because the particles are small (from

<sup>†</sup> Email address for correspondence: [dbb@utc.fr](mailto:dbb@utc.fr)

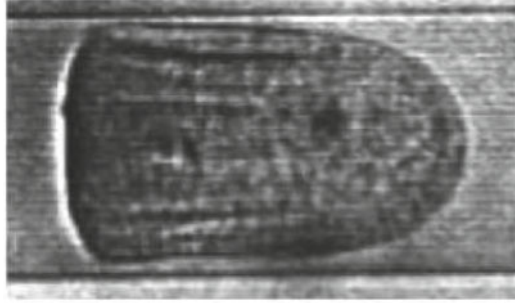


FIGURE 1. Large initially spherical capsule with a cross-linked ovalbumin membrane, flowing in a cylindrical pore (diameter  $75\ \mu\text{m}$ ). Folds appear on the side of the capsule where the membrane is under compression. Image obtained with the experimental method of Lefebvre *et al.* (2008).

a few micrometres to a few millimetres) and fragile. Large capsules with dimensions of a few millimetres can be squeezed between two parallel plates (Carin *et al.* 2003; Risso & Carin 2004). The squeezing force and the overall capsule deformation are measured simultaneously. The interpretation of the results in terms of the membrane mechanical properties necessitates a good mechanical model of the process, as it can involve large deformations of the capsule with reversible reduction of diameter as large as 70%. For very small capsules with dimensions of a few micrometres, it is possible to use the same measurement principle with atomic force microscopy (Fery & Weinkamer 2007). However, the method is difficult to use and must be applied to a number of capsules to get an average value for a population.

A simple way to test a population of capsules is to flow a capsule suspension in a small pore which has transversal dimensions comparable with those of the suspended capsules (Lefebvre *et al.* 2008; Chu *et al.* 2010). The hydrodynamic stresses and the constraints due to the channel walls cause large deformations of the capsules that depend on the flow strength and on the particle intrinsic physical properties such as relative size compared with the channel section and membrane constitutive behaviour. The capsule deformation, volume and velocity can be measured simultaneously by means of image analysis. A sophisticated model of the flow of a capsule in a small pore then allows us to infer the membrane mechanical properties from the experimental results. The feasibility of the method has been demonstrated for millimetre size capsules (Risso, Collé-Paillet & Zagzoule 2006; Lefebvre & Barthès-Biesel 2007) and for micrometre size capsules (Lefebvre *et al.* 2008; Chu *et al.* 2010). In both cases, the capsules were initially spherical with a membrane made of alginate cross-linked with either human serum albumin (HSA) or ovalbumin for the millimetre or micrometre size particles, respectively. The model used to analyse the experiments considered the flow of a centred spherical capsule in a cylindrical channel. The situation is thus fully axisymmetric. This allows integration of the different quantities (stress, deformation, etc.) in the azimuthal direction, so that the problem equations need only to be solved in a meridian plane. The simplification is significant.

However, observations of large capsules flowing in a cylindrical pore indicate that folds occur on the membrane as shown in figure 1. The presence of such folds means that the deformation of the membrane is not axisymmetric but three-dimensional (3D). Then the question which arises is how accurate (or inaccurate) is the axisymmetric

model used to analyse the deformation of a spherical capsule in a cylindrical pore. In order to answer this question a 3D model of this flow must be devised.

A related problem is the flow of a capsule in a microfluidic pore. When such pores are created by means of soft lithography techniques, they have a rectangular or square cross-section. The flow of an initially spherical capsule in a pore with a square or rectangular cross-section is obviously 3D. A new model is thus necessary to analyse the deformation of the capsule in terms of the membrane properties. This situation is quite interesting to study as there is an increasing interest for designing micro-encapsulation systems inside microfluidic devices (Zhang *et al.* 2006; Huang *et al.* 2007; Yeh *et al.* 2009). Creating a characterization system that can be mounted on-line on the capsule fabrication device would be very useful to test and sort the particles.

In this paper, we study the 3D flow of an initially spherical simple capsule consisting of a liquid drop enclosed by a very thin hyperelastic membrane. We assume that the flow Reynolds number is small and we adapt the numerical method of Walter *et al.* (2010) to model the fluid–structure interaction and the confining effect of the solid boundaries: the fluid motion is solved by means of the boundary integral (BI) method, while the membrane mechanics is solved by means of a finite element (FE) method. The coupling of the two methods has been shown to be very precise and to remain numerically stable even when the membrane is subjected to compressive forces causing buckling.

The method used to simulate the fluid–structure interactions occurring when a spherical capsule flows in a pore of various cross-sections is detailed in §2. We then study the 3D evolution and deformation of a capsule in a cylindrical pore and compare the results with the ones obtained with the largely used axisymmetric numerical model in §3. In §4, we model the flow of a spherical capsule in a square-section pore, give new results on the effect of size ratio and flow strength and show how these can be used to analyse experimental measurements of initially spherical capsules flowing in such pores. We conclude with a critical analysis and comparison of the two set-ups.

## 2. Problem statement and numerical method

The flow configuration is similar to the axisymmetric case studied by Quéguiner & Barthès-Biesel (1997), Diaz & Barthès-Biesel (2002) and Lefebvre & Barthès-Biesel (2007) or to the 3D situation considered by Pozrikidis (2005), Doddi & Bagchi (2008) and Kuriakose & Dimitrakopoulos (2011); it will be only summarized in the following.

### 2.1. Problem description

The channel consists of a long prismatic tube with constant cross-section with characteristic dimension  $\ell$ . Entrance and exit effects are neglected. As indicated in figure 2, we consider either a cylindrical tube with a circular section of radius  $R$  ( $\ell = R$ ) or a microfluidic channel with a square section of side  $h$  ( $\ell = h/2$ ). The channel is filled with an incompressible Newtonian liquid of viscosity  $\mu$  flowing with mean velocity  $V$  and flow rate  $Q$ . The velocity field in the channel in absence of particle is denoted  $v^\infty$ .

The capsule is initially spherical with radius  $a$ . It is filled with a Newtonian incompressible liquid with viscosity  $\lambda\mu$  and enclosed by an infinitely thin impermeable hyperelastic membrane with surface shear elastic modulus  $G_s$  and area dilatation modulus  $K_s$ . Buoyancy forces are neglected and consequently, when the capsule is centred on  $Oz$ , it remains centred. However, if the capsule were not

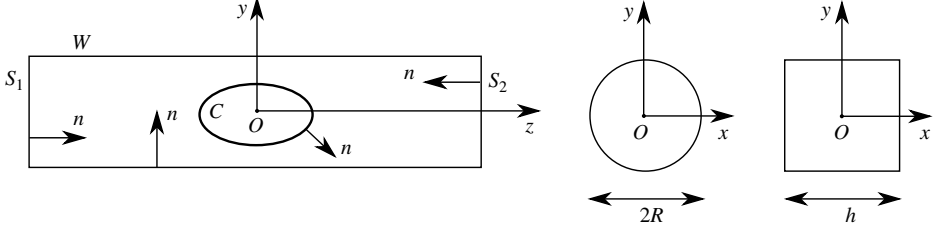


FIGURE 2. Prismatic channel with axis  $Oz$ . The cross-section is either circular with radius  $R$  or square with side  $h$ .

centred on the tube axis, it would migrate towards it (Helmy & Barthès-Biesel 1982; Pozrikidis 2005; Doddi & Bagchi 2008). We use a reference frame  $Oxyz$ , centred at time  $t$  on the capsule centre of mass  $O$ ,  $Oz$  being along the tube axis (figure 2). We are interested in the steady deformed state of the capsule in the tube. The membrane velocity is then zero (because of the flow symmetry) and the internal fluid at rest. Consequently the internal viscosity value does not influence the steady deformation and we can take  $\lambda = 1$  without loss of generality. Of course,  $\lambda$  has an influence on the time it takes to reach the steady state (Diaz & Barthès-Biesel 2002).

The flow Reynolds number is assumed to be very small so that the internal and external liquid motion satisfies the Stokes equations. We solve these in a domain bounded by the cross-sections  $S_1$  at the entrance and  $S_2$  at the exit, that are both located far enough from  $O$  for the capsule flow perturbation to vanish. The other domain boundaries are the channel wall  $W$  and the capsule surface  $C$ . The unit normal vector  $\mathbf{n}$  to all of the boundaries points inwards the suspending liquid. We use  $\mathbf{v}^{(\beta)}$ ,  $\boldsymbol{\sigma}^{(\beta)}$  and  $p^{(\beta)}$  to denote the velocity, stress and pressure fields in the suspending ( $\beta = 1$ ) and internal ( $\beta = 2$ ) liquids.

The problem boundary conditions are:

(a) no flow disturbance on  $S_1$  and  $S_2$  as they are far from the capsule:

$$\mathbf{v}^{(1)}(\mathbf{x}, t) \rightarrow \mathbf{v}^\infty(\mathbf{x}), \quad \mathbf{x} \in S_1 \cup S_2; \quad (2.1)$$

(b) pressure values prescribed on  $S_1$  and  $S_2$ :

$$p^{(1)}(\mathbf{x}, t) = 0, \quad \mathbf{x} \in S_1, \quad (2.2)$$

$$p^{(1)}(\mathbf{x}, t) = \Delta P(t) + \Delta P^\infty, \quad \mathbf{x} \in S_2, \quad (2.3)$$

where  $\Delta P^\infty$  is the undisturbed pressure drop between  $S_1$  and  $S_2$  in the absence of capsule and  $\Delta P$  is the additional pressure drop due to the capsule;

(c) no slip on the channel wall  $W$ :

$$\mathbf{v}^{(1)}(\mathbf{x}, t) = \mathbf{0}, \quad \mathbf{x} \in W; \quad (2.4)$$

(d) no slip on the capsule deformed surface  $C$ :

$$\mathbf{v}^{(1)}(\mathbf{x}, t) = \mathbf{v}^{(2)}(\mathbf{x}, t) = \frac{\partial}{\partial t} \mathbf{x}(X, t), \quad \mathbf{x} \in C, \quad (2.5)$$

where  $X$  denotes the initial position of a membrane material point located at position  $\mathbf{x}$  at time  $t$ ;

(e) the load  $\mathbf{q}$  on the membrane is due to the viscous traction jump:

$$(\boldsymbol{\sigma}^{(1)} - \boldsymbol{\sigma}^{(2)}) \cdot \mathbf{n} = \mathbf{q}, \quad \mathbf{x} \in C. \quad (2.6)$$

## 2.2. Capsule membrane mechanics

When the thickness of a capsule membrane is small compared with the capsule dimensions and typical radius of curvature, the membrane can be modelled as a hyperelastic surface devoid of bending resistance. A membrane material point, identified by its position  $\mathbf{X}$  in the reference state, is displaced to the position  $\mathbf{x}(\mathbf{X}, t)$  in the deformed state. Because the bending stiffness is neglected, the normal vector to the surface remains normal during deformation. The local deformation of the surface is measured by the Green–Lagrange strain tensor

$$\mathbf{e} = \frac{1}{2}(\mathbf{F}^T \cdot \mathbf{F} - \mathbf{I}), \quad (2.7)$$

where  $\mathbf{F} = \partial \mathbf{x} / \partial \mathbf{X}$ . The membrane deformation can also be quantified by the principal dilatation ratios  $\lambda_1$  and  $\lambda_2$  in its plane which correspond to eigenvalues of  $\mathbf{e}$ . Since the membrane is infinitely thin, elastic stresses are replaced by a Cauchy tension tensor  $\boldsymbol{\tau}$  corresponding to forces per unit arclength measured in the plane of the membrane.

A number of constitutive laws are available to model thin hyperelastic membranes (Barthès-Biesel, Diaz & Dhenin 2002). Different material behaviours can be described for large deformation, including the strain-softening behaviour of gelled membranes exhibiting rubber-like elasticity or the strain-hardening behaviour of membranes made of a polymerized network with strong covalent links. For conciseness, we will restrict the study to the widely used neo-Hookean (NH) law, which has been found to be the appropriate law to model the behaviour of protein-reticulated membranes (Carin *et al.* 2003; Lefebvre *et al.* 2008; Chu *et al.* 2010). The NH law describes the behaviour of an infinitely thin sheet of a 3D isotropic and incompressible material. The principal tensions are given by

$$\tau_1 = \frac{G_s}{\lambda_1 \lambda_2} \left[ \lambda_1^2 - \frac{1}{(\lambda_1 \lambda_2)^2} \right] \quad (\text{likewise for } \tau_2). \quad (2.8)$$

The hypothesis of volume incompressibility implies that area dilatation is balanced by membrane thinning and correspondingly the area dilatation modulus is  $K_s = 3G_s$ .

Owing to the negligible inertia of a membrane with small thickness, the membrane motion is governed by the local equilibrium equation

$$\nabla_s \cdot \boldsymbol{\tau} + \mathbf{q} = \mathbf{0}, \quad (2.9)$$

where  $\mathbf{q}$  is the external load exerted by the fluids as given by (2.6) and  $\nabla_s \cdot$  is the surface divergence operator in the deformed configuration.

Since the bending modulus of the membrane has been neglected, the capsule wall buckles locally in the regions where the elastic tensions are compressive (see, for example, Cerda & Mahadevan 2003, Luo & Pozrikidis 2007 and Finken & Seifert 2006). In order to study the post-buckling behaviour of the capsule, bending moments and transverse shear forces must be added to (2.9) and a constitutive equation must be postulated to relate bending moments and local deformations. It follows that the bending behaviour of a capsule is a complicated problem of shell mechanics that is not completely resolved yet.

The simplified membrane model that we use here will be appropriate to model capsules with a very low bending resistance. It will detect zones where tensions are compressive but cannot compute the post-buckling behaviour of the capsule.

## 2.3. Numerical procedure

We use the method developed by Walter *et al.* (2010) which is based on the coupling of a membrane FE method (for the capsule wall mechanics) and a boundary integral method (for the internal and external flows). We position the capsule on the channel axis and then follow the position of the material points of the membrane after the start of flow at time  $t = 0$ . At each time step, the deformation of the capsule may be computed from the position of the membrane material points. The elastic tension tensor  $\boldsymbol{\tau}$  is then obtained from the values of the in-plane stretch ratios  $\lambda_1$  and  $\lambda_2$ . The FE method used to solve the equilibrium of the membrane provides the load  $\mathbf{q}$ .

The Stokes equations are recast in boundary integral form for the 3D motion of the internal and external fluids. In the case of a capsule in a tube and for  $\lambda = 1$ , the velocity  $\mathbf{v}(\mathbf{x})$  of any point  $\mathbf{x}$  in the fluid domain is given by Pozrikidis (2005)

$$\mathbf{v}(\mathbf{x}) = \mathbf{v}^\infty(\mathbf{x}) - \frac{1}{8\pi\mu} \left[ \int_C \mathbf{J}(\mathbf{r}) \cdot \mathbf{q} \, dS(\mathbf{y}) + \int_W \mathbf{J}(\mathbf{r}) \cdot \mathbf{f} \, dS(\mathbf{y}) - \Delta P \int_{S_2} \mathbf{J}(\mathbf{r}) \cdot \mathbf{n} \, dS(\mathbf{y}) \right], \quad (2.10)$$

where  $\mathbf{f}$  is the disturbance wall friction due to the capsule and  $\mathbf{r} = \mathbf{y} - \mathbf{x}$ . The Green kernel is defined by

$$\mathbf{J}(\mathbf{r}) = \frac{1}{r} \mathbf{I} + \frac{\mathbf{r} \otimes \mathbf{r}}{r^3}, \quad (2.11)$$

where  $r = \|\mathbf{r}\|$  and  $\mathbf{I}$  is the identity tensor.

Applying the reciprocal theorem to the flow without capsule ( $\mathbf{v}^\infty, \boldsymbol{\sigma}^\infty$ ) and to the flow with the capsule ( $\mathbf{v}^{(1)}, \boldsymbol{\sigma}^{(1)}$ ) in the domain bounded by  $S_1 \cup S_2 \cup W \cup C$ , we find

$$\int_C [\boldsymbol{\sigma}^{(1)} \cdot \mathbf{n}] \cdot \mathbf{v}^\infty \, dS - (\Delta P + \Delta P^\infty)Q = \int_C [\boldsymbol{\sigma}^\infty \cdot \mathbf{n}] \cdot \mathbf{v}^{(1)} \, dS - \Delta P^\infty Q, \quad (2.12)$$

where we have used the facts that the flow rate  $Q$  is the same with and without the capsule and that the velocity is zero on  $W$ . Now, we apply the reciprocal theorem to ( $\mathbf{v}^\infty, \boldsymbol{\sigma}^\infty$ ) and to ( $\mathbf{v}^{(2)}, \boldsymbol{\sigma}^{(2)}$ ) in the domain bounded by  $C$

$$\int_C [\boldsymbol{\sigma}^{(2)} \cdot \mathbf{n}] \cdot \mathbf{v}^\infty \, dS = \int_C [\boldsymbol{\sigma}^\infty \cdot \mathbf{n}] \cdot \mathbf{v}^{(2)} \, dS. \quad (2.13)$$

We subtract (2.12) and (2.13) and use (2.5) and (2.6) to find that the additional pressure drop is simply given by

$$\Delta P = \frac{1}{Q} \int_C \mathbf{v}^\infty(\mathbf{x}) \cdot \mathbf{q} \, dS(\mathbf{y}). \quad (2.14)$$

Once the value of the pressure disturbance  $\Delta P$  is known, the application of (2.10) to  $\mathbf{x} \in W$

$$0 = \int_C \mathbf{J}(\mathbf{r}) \cdot \mathbf{q} \, dS(\mathbf{y}) + \int_W \mathbf{J}(\mathbf{r}) \cdot \mathbf{f} \, dS(\mathbf{y}) - \Delta P \int_{S_2} \mathbf{J}(\mathbf{r}) \cdot \mathbf{n} \, dS(\mathbf{y}) \quad (2.15)$$

yields an implicit equation for  $\mathbf{f}$  which is solved numerically. Applying then (2.10) to  $\mathbf{x} \in C$ , we obtain the new velocity  $\mathbf{v}(\mathbf{x}, t)$  of the membrane points from which we deduce the velocity  $\mathbf{v}(\mathbf{O}, t)$  of the centre of mass. The no-slip equation (2.5) is first

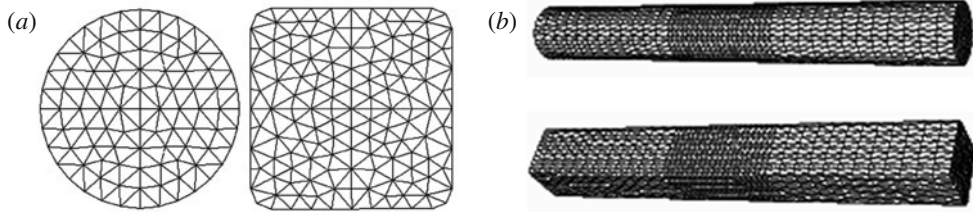


FIGURE 3. (a) Meshes of the circular and square cross-sections; (b) meshes of the prismatic tubes.

modified to keep the centre of mass fixed at point  $O$

$$\mathbf{v}^{(1)}(\mathbf{x}, t) - \mathbf{v}(O, t) = \frac{\partial}{\partial t} \mathbf{x}(X, t), \quad \mathbf{x} \in C. \quad (2.16)$$

Equation (2.16) is then time-integrated to provide the new position of the membrane points. The procedure is repeated until a steady state is reached (typically when the surface of the capsule varies by less than  $5 \times 10^{-4} \times (4\pi a^2)$  over a non-dimensional time  $Vt/\ell = 1$ ).

#### 2.4. Discretization

The surface of the capsule is discretized using triangular curved  $P_2$  elements, which have six nodes (one at each vertex and at the middle of each side) and are associated with quadratic shape functions. The mesh of the initial spherical capsule is obtained by first inscribing an icosahedron (regular polyhedron with 20 triangular faces) in the sphere and subdividing the elements sequentially until the desired number of elements is reached (Ramanujan & Pozrikidis 1998; Walter *et al.* 2010). For all of the 3D computations, we use a capsule mesh with 1280 elements and 2562 nodes, which correspond to a characteristic mesh size  $\Delta h_c = O(0.1a)$ .

The tube mesh is generated using Modulef (INRIA Rocquencourt, France). We first generate the two-dimensional geometry of the tube cross-section with the desired shape (circular or square in the present case). The circular or square cross-sections are meshed with unstructured triangular elements having a mesh size  $\Delta h_s = O(0.14\ell)$ . The corners of the rectangular cross-section have been rounded with an arc (radius  $\Delta h_s$ ) in order to avoid corner effects when solving for the flow (figure 3a). As shown in figure 3(b), the central section of the tube (of length  $4\ell$ ) has a more refined mesh ( $\Delta h_w = O(0.14\ell)$ ) than the inlet and outlet tube sections ( $\Delta h_w = O(0.22\ell)$ ), each of length  $6\ell$ . Altogether, the mesh comprises 1505 nodes and 2976 elements for the cylindrical tube and 1905 nodes and 3768 elements for the rectangular tube.

The numerical method is conditionally stable if the time step satisfies a similar condition to that found for the unbounded case (Walter *et al.* 2010)

$$\frac{V}{\ell} \Delta t < O\left(\frac{\Delta h_c}{\ell} Ca\right), \quad (2.17)$$

where  $\Delta t$  is the time step. All of the results shown hereafter have been obtained with a time step  $V\Delta t/\ell = 5 \times 10^{-5}$ . We have checked the influence of the wall and exit mesh size using a mesh size twice as small as that described above and have not found any significant influence on the capsule deformed profile. This confirms that the error on the capsule shape is mainly determined by the capsule mesh size and is then  $O(\Delta h_c^4)$  as shown by Walter *et al.* (2010).

### 2.5. Case $a/\ell > 1$

When the capsule initial size is larger than the channel cross-dimension, we pre-deform the capsule into an spheroid that fits inside the pore. Correspondingly, a point initially located at  $X, Y, Z$  on the capsule surface is displaced to  $x, y, z$ , such that

$$z = k_1 Z, \quad y = k_2 Y, \quad x = k_2 X, \quad (2.18)$$

with  $k_2^2 k_1 = 1$ , in view of the volume conservation requirement. We choose  $k_2$  such that  $y/\ell = 0.9$ , in order to leave a reasonably thick liquid film between the membrane and the channel wall. The resulting elastic tensions in the membrane and the load  $\mathbf{q}$  exerted on the fluid are computed by means of the FE method. The capsule deformation is then followed in time as explained above. We have verified that the amount of pre-deformation does not influence the results: exactly the same results have been obtained with another value of  $k_2$  such that the capsule is pre-deformed to  $y/\ell = 0.8$ .

### 2.6. Presentation of the results

The model parameters are the capillary number  $Ca = \mu V/G_s$ , which measures the ratio between the viscous and elastic forces and the size ratio  $a/\ell$ . The deformed profile intersections with the  $yz$ - or  $xz$ -planes are determined. These correspond to what is typically observed experimentally for a capsule flowing in a pore. The principal tensions along the profile are also computed in order to detect the presence of compression zones. The position of a point  $M$  on the profile is determined by the angle  $\theta = (\mathbf{e}_z, \mathbf{OM})$ .

## 3. Flow of a capsule in a cylindrical pore

We now consider a pore with a circular cross-section of radius  $R$ . The undisturbed velocity is

$$\mathbf{v}^\infty = 2V[1 - (x^2 + y^2)/R^2]\mathbf{e}_z. \quad (3.1)$$

If we assume the capsule profile to remain axisymmetric, the flow is also axisymmetric and it is possible to integrate (2.9), (2.10), (2.14) and (2.15) analytically in the azimuthal direction. The surface integrals on  $C$  and  $W$  then become line integrals along the meridian curves of the corresponding surfaces, while the integral on  $S_2$  is taken along a radius of the section (Pozrikidis 1992; Quéguiner & Barthès-Biesel 1997; Diaz & Barthès-Biesel 2002; Lefebvre & Barthès-Biesel 2007). With this procedure, a negative azimuthal tension may compress part of the capsule membrane without creating any numerical instability. However, it must be recognized that the solution thus obtained is mechanically unstable: the membrane should actually buckle in these regions as observed experimentally (figure 1).

In the axisymmetric model we use, the tube entrance is shaped as an hyperboloid (Quéguiner & Barthès-Biesel 1997; Diaz & Barthès-Biesel 2002; Lefebvre & Barthès-Biesel 2007). An undeformed capsule is positioned in the entrance section, far enough from the cylindrical part of the pore to fit in, and we follow the entrance process into the cylindrical pore until a steady state is reached. Charts of the capsule deformation parameters as functions of the size ratio, capillary number and osmotic pre-swelling may be found in Lefebvre & Barthès-Biesel (2007), Lefebvre *et al.* (2008) and Chu *et al.* (2010).

### 3.1. Three-dimensional effects on capsule deformation

We compare the results obtained with the 3D computation, where no specific assumption on the problem symmetry is made *a priori*, with those provided by the

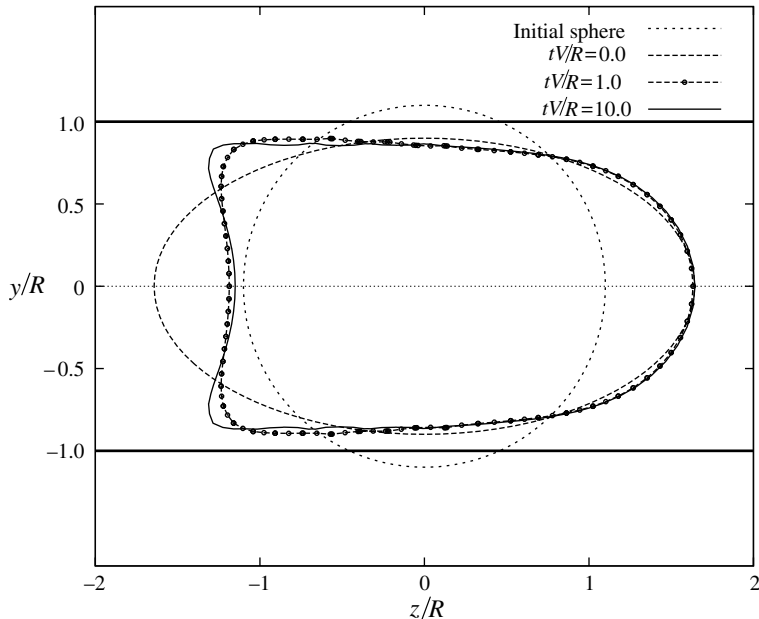


FIGURE 4. Successive profiles of a capsule of aspect ratio  $a/R = 1.1$ , subjected to a capillary number  $Ca = 0.05$ . The initially spherical capsule being larger than the pore is deformed into an ellipsoid at dimensionless time  $tV/R = 0$ . The capsule is then left free to adapt its shape to the flow. It has a steady parachute shape at  $tV/R = 10$ .

axisymmetric model. For the 3D computation, we first stretch the capsule as explained in §2.5 and then let it reach an equilibrium, if any. Results are presented for a typical case where  $a/R = 1.1$  and  $Ca = 0.05$ . It is a deliberate choice to show results for a large capsule aspect ratio, as the larger the aspect ratio the larger the capsule deformation for a given capillary number. The successive capsule profiles are shown in figure 4. We note that the largest shape change occurs at the rear where the curvature evolves from a positive to a negative value. At steady state, the internal liquid being at rest, the internal pressure is constant. In order to adapt to the viscous pressure drop occurring in the external liquid, the membrane curvature must be larger at the front than at the rear, thus leading to slug or parachute shapes of the capsule.

As shown in figure 5(a), the meridional axisymmetric and 3D profiles are almost superimposed in plane  $Oyz$ . The cross-profiles in plane  $z = 0$  are also superimposed notwithstanding small oscillations of the 3D profile about the mean circular profile predicted by the axisymmetric model (figure 5b).

The axisymmetric computation shows that the principal tension  $\tau_2$  in the azimuthal direction is negative, and thus compressive, on part of the membrane (for  $\theta/\pi \in \pm[0.35; 0.8]$  or  $z \in [-1.16; 0.43]$ ) as shown in figure 6. This means that in the grey area of figure 5(a), the membrane is undergoing compression and will tend to buckle. In this area where the membrane is undergoing compression and where there is no bending resistance to regulate the process, the 3D model leads to values of  $\tau_2$  which oscillate about zero with a wavelength of the order of twice the grid spacing. The membrane undergoes a numerical buckling which mimics the actual one qualitatively only. We have checked that the wavelength of the oscillation decreases by a factor two when the number of elements is doubled.

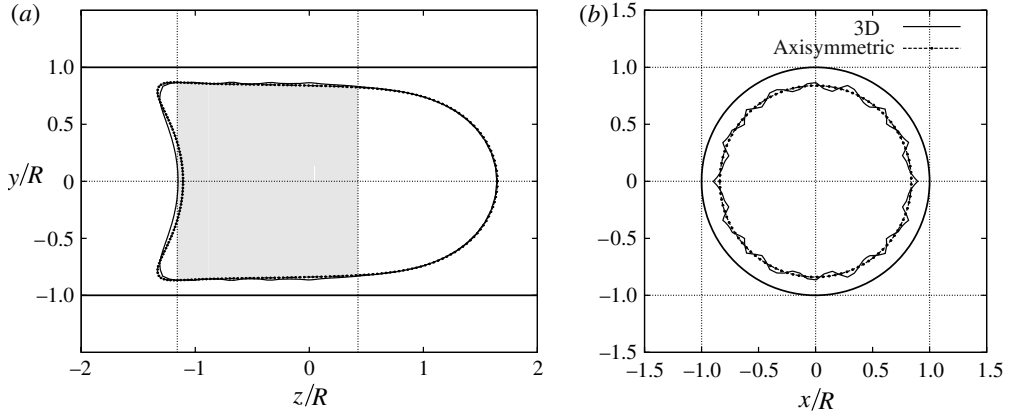


FIGURE 5. Comparison of the capsule profiles at steady state obtained with the axisymmetric and 3D computations for  $a/R = 1.1$  and  $Ca = 0.05$ . (a) Profiles in the  $yz$ -plane: the zone where compression occurs is shaded in grey; (b) cross-profiles in the  $xy$ -plane for which  $z = 0$ : the oscillation of the 3D profile indicate a tendency towards folding.

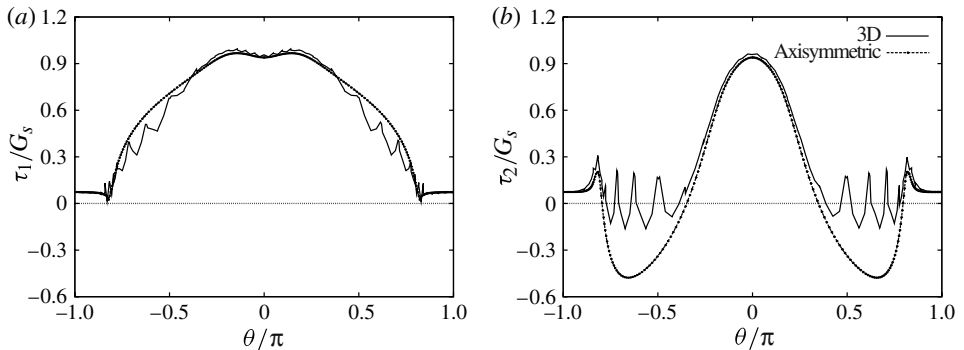


FIGURE 6. Comparison of the principal tensions in the  $yz$ -plane at steady state obtained with the axisymmetric and 3D computations for  $a/R = 1.1$  and  $Ca = 0.05$ . The principal tensions are plotted as a function of position  $\theta/\pi$  along the profile. Tension  $\tau_1$  is directed along the profile, while  $\tau_2$  is perpendicular to the plane and thus in the hoop direction.

As a consequence of the compression, the 3D cross-profile in plane  $z = 0$  undergoes small oscillations about the mean circular profile predicted by the axisymmetric model (figure 5b). These oscillations correspond qualitatively to the folds that are observed experimentally and whose wavelength is obviously regulated by the membrane thickness and bending stiffness. The values of the principal tension  $\tau_1$  along a ‘meridian’ curve in the  $Oyz$  plane also oscillate about the axisymmetric value.

Finally we note that on the part of the membrane where no compression occurs (i.e. about the front of the capsule), the tensions values are superimposed. In particular, the maxima of  $\tau_1$  are identical with the two computations. This indicates that the axisymmetric and 3D model would both lead to the same mechanical failure criterion.

In conclusion, we find that, for large capsule aspect ratios, there is significant lateral compression on the capsule membrane leading to folds similar to those observed experimentally and shown in figure 1. For smaller values of the size ratio  $a/R$ , we

obtain the same qualitative results, namely that the axisymmetric and 3D profiles are almost identical. The fit is optimal for small aspect ratios and capillary numbers, as the capsule is then devoid of compression zones around its surface at steady state.

The axisymmetric model predicts that for a given size ratio, there exists a higher bound on the capillary number  $Ca_{max}$  for which it is possible to reach a steady equilibrium state (Chu *et al.* 2010). For flow rates such that  $Ca > Ca_{max}$  the capsule undergoes continuous extension. This phenomenon is similar to that which occurs in elongational flow for NH membranes and which is due to the strain-softening behaviour of the NH law (Barthès-Biesel 2011). The 3D computation also finds an upper bound on the values of  $Ca$  for which it is not possible to obtain a steady state. The values of  $Ca_{max}$  are about 10% larger with the 3D model than with the axisymmetric model. This difference may be attributed to the numerical technique and to the discretization of the membrane. As a consequence, the exact 3D value of  $Ca_{max}$  is immaterial, and the upper bounds given by Chu *et al.* (2010) can be used for practical purposes.

### 3.2. Conclusion for the capsule flow in a cylindrical pore

The axisymmetric model has been used by Lefebvre *et al.* (2008) and Chu *et al.* (2010) to analyse experiments on microcapsules flowing in a cylindrical pore of known radius  $R$ . The procedure is based on the contour extraction of the deformed profile from which the capsule volume and size ratio  $a/R$  are computed. A database of computed deformed profiles obtained for different values of  $a/R$  and  $Ca$  is then searched to find the same deformation characteristics as the experimentally observed profile. This leads to a set of values of  $Ca$  from which  $G_s$  is inferred (for details, see Lefebvre *et al.* 2008 and Chu *et al.* 2010).

We have shown that although the capsule membrane tends to fold, the axisymmetric profiles represent a very good approximation of the actual 3D profiles. It follows that the characterization procedure based on the axisymmetric model is sound. As regards the elastic tensions though, the axisymmetric model can only be used to evaluate their maximum values and determine the zones where buckling will occur. This is an important result, as it is much easier and faster to use an axisymmetric representation than a full 3D representation. For example, for  $Ca = 0.05$  and  $a/l = 0.9$ , the computation of a time interval  $tV/\ell = 1$  takes 1 h for the axisymmetric case using one core of a 128-core cluster and 5.7 h for the 3D case using 8 cores (of course, those times are given for a usual mesh size, but increase with the mesh refinement).

## 4. Flow in a square cross-section pore

The uniform axial velocity distribution  $\mathbf{v}^\infty = v^\infty(x, y)\mathbf{e}_z$  in a duct with a square cross-section is given in a number of textbooks (e.g. Pozrikidis 1997)

$$v^\infty(x, y) = \frac{\pi V \sum \left[ \frac{1}{n^3} - \frac{\cosh n\pi x/h}{n^3 \cosh n\pi/2} \right] \sin n\pi(y/h + 1/2)}{2 \left[ \frac{\pi^4}{96} - \sum \frac{\tanh n\pi/2}{n^5 \pi/2} \right]} \quad n = 1, 3, \dots \quad (4.1)$$

where the sums are taken over odd values of  $n$ . When applying the no-slip condition (2.15), we set to zero the velocity of the node point located in the middle of the rounded corner (figure 3), where its actual value is  $0.05V$  or  $0.02V$  for the standard or refined boundary mesh, respectively. As the change in wall mesh size has a negligible influence on the capsule profile, we consider that this corner rounding leads to a

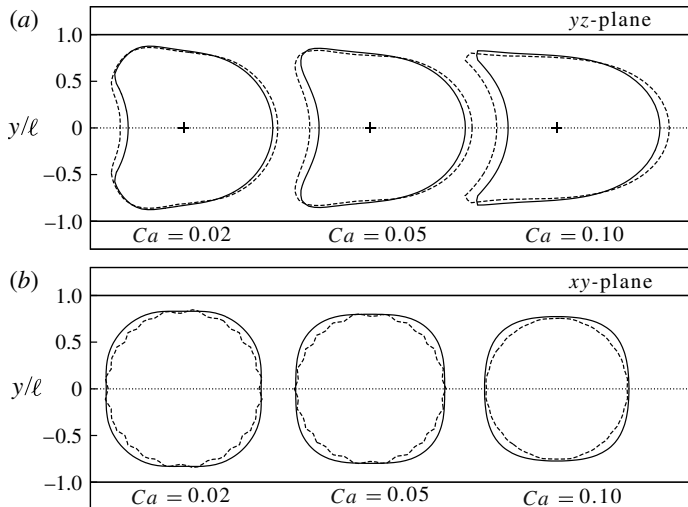


FIGURE 7. Steady capsule profiles in a square channel (full line) and in a cylindrical tube (dashed line) for  $a/\ell = 0.9$ . (a) Profiles in the  $yz$ -plane, with the cross on the axis indicating the position of the centre of mass  $z = 0$ ; (b) cross-profiles in the  $xy$ -plane for which  $z = 0$ .

negligible error. In the following, we analyse the influence of the confinement induced by a square tube as compared to a cylindrical tube. For brevity, we use the notation ‘circular capsule’ or ‘square capsule’ for the capsule in the circular or square section pore, respectively. The results shown for the circular capsule are obtained with the three-dimensional model.

#### 4.1. Case $a/\ell < 1$

We first consider the case  $2a/h = 0.9$  where the capsule is only slightly smaller than the channel. The longitudinal and cross-profiles are shown in figure 7 and compared with the three-dimensional profiles obtained in a cylindrical tube for the same values of  $Ca$  and  $a/R$ . We note that for small capillary numbers (e.g.  $Ca = 0.02$ ) the deformation is small and the deformed profiles in the two channels are almost superimposed. When  $Ca$  increases, the circular capsule having less room to deform is more elongated than the square capsule, which can expand in the corners of the channel as shown in figure 7(b). As a consequence, the deformed profile of a square capsule is not axisymmetric. Another consequence is that the tension  $\tau_1$  along the profile is larger for the circular than for the square capsule as shown in figure 8(a). Furthermore, the cross-section of the square capsule is not under compression ( $\tau_2$  is positive everywhere), whereas the circular capsule is compressed and tends to buckle as discussed in the previous section (figure 8b). For  $Ca = 0.1$ , one could be under the wrong impression that the circular capsule does not buckle: actually, it buckles for negative values of  $z$ .

#### 4.2. Case $a/\ell \geq 1$

We now turn to large capsules that must be pre-deformed. The longitudinal and cross-profiles are shown in figure 9 for the case  $a/\ell = 1.1$ . First we note that for low flow strength ( $Ca \leq 0.05$ ), the square capsule membrane is compressed near the wall but is extended in the corners. By contrast, the circular capsule is compressed all around as evidenced by the cross-profiles (figure 9b) and by the corresponding oscillations

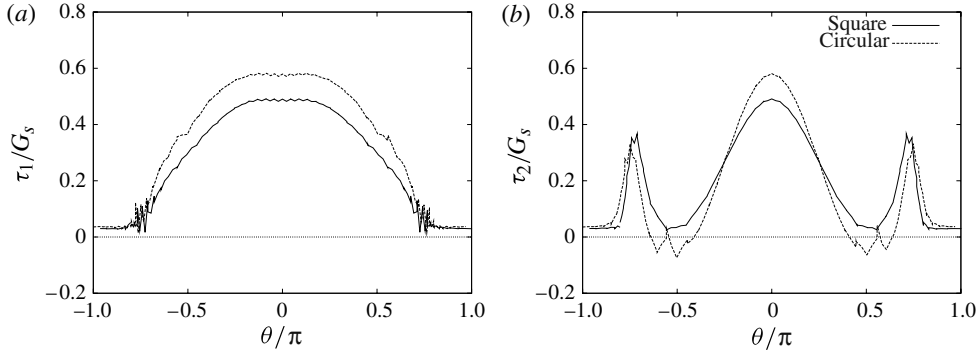


FIGURE 8. Principal tensions in the  $yz$ -plane at steady state for a capsule ( $a/\ell = 0.9$ ) flowing in a cylindrical or square channel at  $Ca = 0.05$ . The principal tensions are plotted as a function of position  $\theta/\pi$  on the profile.

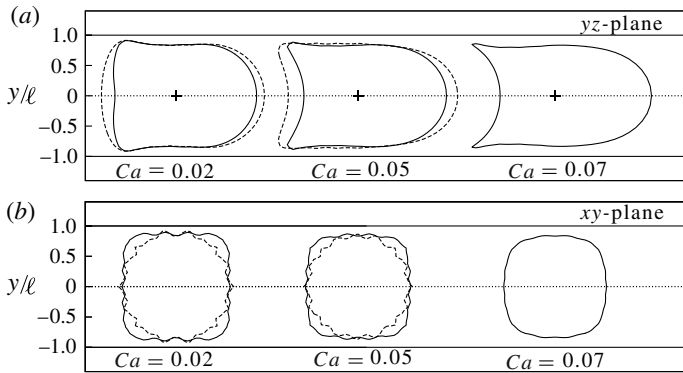


FIGURE 9. Steady capsule profiles in a square channel (full line) and in a cylindrical tube (dashed line) for  $a/\ell = 1.1$ . (a) Profiles in the  $yz$ -plane, with the cross on the axis indicating the position of the centre of mass  $z = 0$ ; (b) cross-profiles in the  $xy$ -plane for which  $z = 0$ .

of tension  $\tau_2$  (figure 10b). As the flow strength increases, the capsule is stretched along the pore axis, the surface area increases and the negative tensions disappear. The circular capsule being more deformed than the square one, the tension level in the membrane is higher as shown in figure 10.

For  $a/\ell = 1.1$  and high flow strength ( $Ca = 0.08$ – $0.09$ ), the capsule also undergoes continuous elongation and no steady equilibrium state can be reached. We note again that the value of  $Ca_{max}$  for which this phenomenon occurs is larger in the square section pore than in the circular section pore. Indeed, in the cylindrical pore, a flow strength  $Ca = 0.07$  exceeds  $Ca_{max}$ , which is the reason why no circular capsule profile is shown in figure 9 for  $Ca = 0.07$ .

#### 4.3. Effect of $Ca$ and $a/l$

From an experimental point of view, it is convenient to characterize the capsule deformation with the maximum profile length  $L$  and the axial length  $L_a$  along the  $Oz$  axis. These two parameters are equal for slug shapes, whereas  $L_a < L$  for parachute shapes. The lengths  $L$  and  $L_a$  are plotted as a function of  $Ca$  in figure 11(a) for the circular and square pores. We find that, to obtain the same elongation  $L$  in the

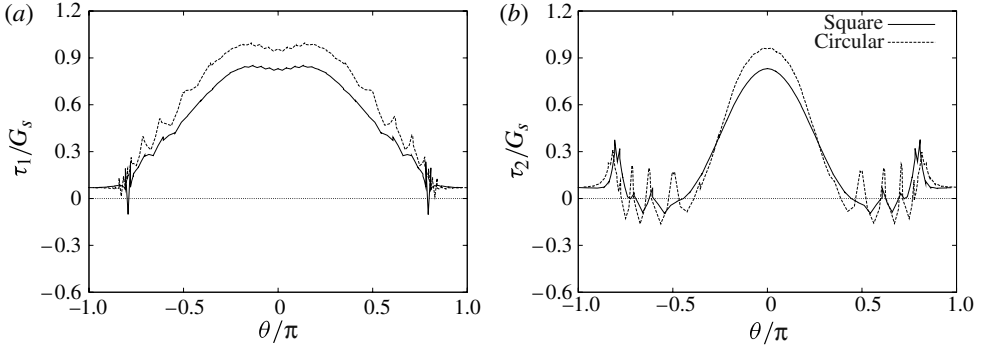


FIGURE 10. Principal tensions in the  $yz$ -plane at steady state for a capsule ( $a/\ell = 1.1$ ) flowing in a cylindrical or square channel at  $Ca = 0.05$ .

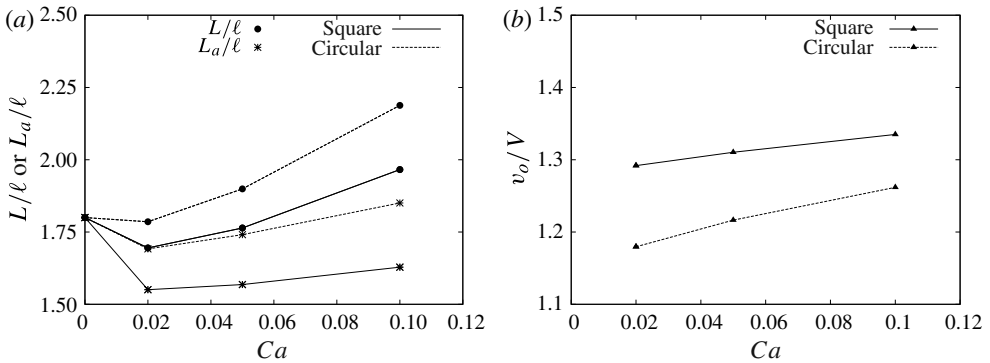


FIGURE 11. Capsule maximum length  $L$ , axial length  $L_a$  and centre of mass velocity  $v_o$  for a capsule ( $a/\ell = 0.9$ ) at steady state flowing in a cylindrical or square channel. For the same value of  $Ca$ , the capsule is more deformed in the cylindrical than in the square pore and travels at a slower speed.

two pores, the value of  $Ca$  in the square pore must be about 60% higher than that in the circular pore. The values of  $L - L_a$  are the same for the two types of pores, as can also be observed from figure 7. The steady velocity of the capsule centre of mass  $v_o$  is plotted in figure 11(b). It is 10% higher in the square than in the circular pore. The explanation for this larger velocity is outlined by Lefebvre *et al.* (2008) and summarized here in the limiting case where the film is thin. When a capsule has the same deformed axial profile in a circular or square channel, it is subjected to the same pressure drop  $\Delta P_c$  along its length  $L$  (because the front and back curvatures are the same). This pressure drop is related to the viscous loss in the lubrication film. For example for the circular tube, a force balance yields

$$\Delta P_c \pi \ell^2 = 2\pi \ell L \mu v_{O_{cyl}} / \bar{h}_{cyl} \quad (4.2)$$

where  $\bar{h}_{cyl}$  is the mean film thickness. The same expression is found for the mean film thickness  $\bar{h}_{sq}$  in terms of the capsule velocity  $v_{O_{sq}}$  in the square channel. It follows that

$$\frac{v_{O_{sq}}}{v_{O_{cyl}}} = \frac{\bar{h}_{sq}}{\bar{h}_{cyl}}. \quad (4.3)$$

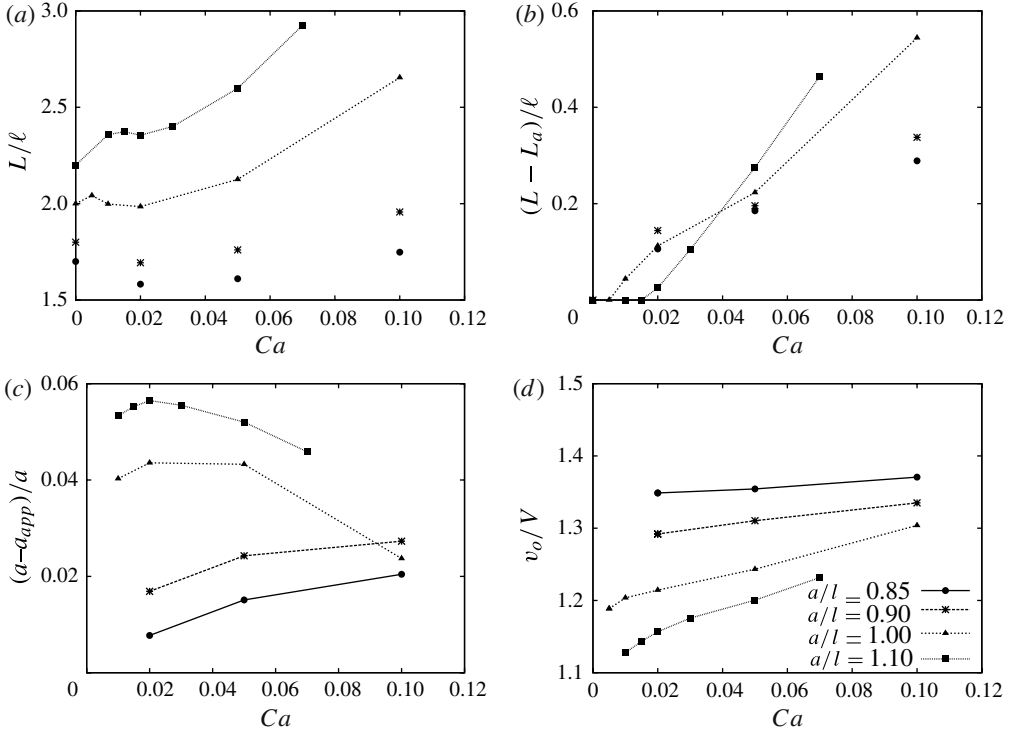


FIGURE 12. Plots of the values of the capsule total length  $L$ , parachute depth  $L - L_a$ , difference between axisymmetric and actual capsule radius and centre of mass velocity  $v_o$ . These graphs are useful to analyse experimental data on capsules flowing in square section pores.

There are two limiting shapes of the capsule cross-section in a square channel that correspond to a given axial profile. If the cross-section of the capsule is square, the mean thickness is constant  $\bar{h}_{sq} = \bar{h}_{cyl}$ . If it is circular with radius  $\ell - \bar{h}_{cyl}$ ,  $\bar{h}_{sq} > \bar{h}_{cyl}$  due to the contribution of the corners. From (4.3), the velocity  $v_{Osq}$  is then equal or larger than  $v_{O cyl}$ . The numerical model finds that the capsule cross-section is square with rounded corners (figures 7b and 9b), which indicates that  $v_{Osq}$  must be larger than  $v_{O cyl}$ .

In conclusion, larger flow rates must be used in the square pore than in the cylindrical pore to get the same deformation. This may cause some experimental difficulties as the capsule will move faster and its detection will be more difficult.

The combined effects of flow strength and aspect ratio are summarized in figure 12. We note that for aspect ratios less than unity, the capsule is first compressed in the axial direction when the capillary number is small (e.g.  $Ca \leq 0.02$ ) as can be surmised from the initial decrease of  $L$ . Then the stretching effect of the viscous forces elongates the capsule. When  $a/\ell \leq 0.95-0.97$  the capsule takes a parachute shape for all values of  $Ca$ . For larger aspect ratios (e.g.  $a/\ell \geq 1$ ), the parachute appears only when  $Ca$  exceeds a critical value  $Ca_c$ . When  $Ca < Ca_c$ , the capsule has a slug shape and  $(L - L_a)/\ell = 0$ . The capsule moves faster than the average fluid velocity as it is centred on the channel. All of these phenomena are qualitatively similar to those observed for the flow of capsules in cylindrical tubes (Lefebvre & Barthès-Biesel 2007; Lefebvre *et al.* 2008) irrespective of the membrane constitutive law.

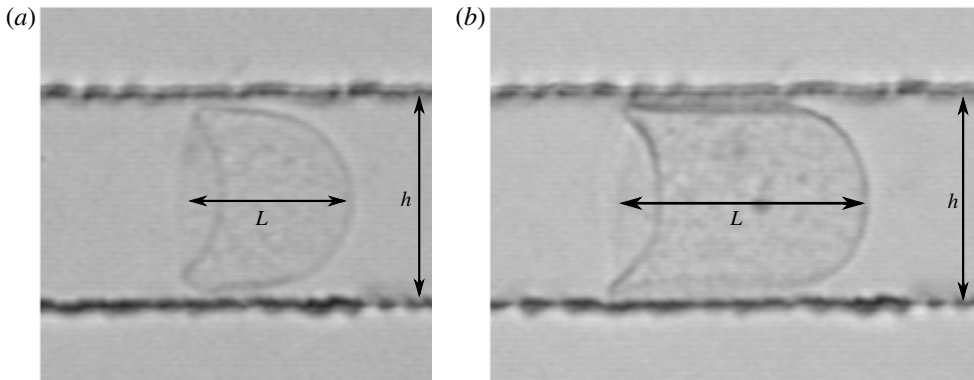


FIGURE 13. Flow of initially spherical capsules with a cross-linked ovalbumin membrane in a  $50\ \mu\text{m} \times 50\ \mu\text{m}$  microfluidic channel; (a)  $a_{app}/\ell = 0.85$ ,  $v_o = 6.6\ \text{mm s}^{-1}$ ; (b)  $a_{app}/\ell = 1.05$ ,  $v_o = 4.5\ \text{mm s}^{-1}$ .

These plots are necessary to analyse the flow of capsules in a square section pore and to infer a value for the membrane elastic modulus from the capsule deformation and velocity. In a typical microfluidic device, only the capsule deformed profile in one plane (e.g. the  $yz$ -plane) can be observed. It is thus difficult to evaluate the volume (or the initial radius) of the capsule. A way to do it is to rotate the profile in the  $yz$ -plane about the pore axis as if the capsule were axisymmetric and to deduce an approximate initial radius  $a_{app}$ , from the pseudo-axisymmetric volume. The model allows us to compute the error between  $a_{app}$  and the real value  $a$ . Indeed, the model yields a steady deformed profile for a capsule of known volume. If we rotate the deformed profile in the  $yz$ -plane about the channel axis and compute the volume of the axisymmetric shape thus obtained, we can infer the numerical value of  $a_{app}$  and compare it to  $a$ . This is done in figure 12(c) where we find that  $a_{app}$  always underestimates  $a$ . This is of course due to the propensity of the square capsule to occupy the tube corners for large aspect ratios: the capsule volume that expands in the corners is not taken into account during the rotation procedure described above.

#### 4.4. Comparison with experimental results

Measurement of the flow of artificial capsules in cylindrical tubes and in square section microfluidic pores have been conducted by Lefebvre *et al.* (2008). The capsules are initially spherical and have a cross-linked ovalbumin membrane. They are suspended in a 100% glycerin solution (viscosity  $\mu = 1\ \text{Pa}$ ) and flowed through microchannels with a cross-section comparable to the capsule,  $a/\ell = O(1)$ . The capsule deformed profile are recorded with a high-speed camera and their velocity is measured. Lefebvre *et al.* (2008) used a NH model to describe the membrane elasticity and found a shear modulus value  $G_s = 0.07 \pm 0.01\ \text{N m}^{-1}$  from the cylindrical pore measurements.

We outline briefly how the results of §4.3 can be used to evaluate the mechanical properties of capsules. In figure 13, we show deformed capsules obtained in a microfluidic channel with a  $50\ \mu\text{m} \times 50\ \mu\text{m}$  cross-section under the same experimental conditions as Lefebvre *et al.* (2008). We first note the qualitative similarity between the profiles of figures 7(a) and 13(a) on the one hand, and of figures 9(a) and 13(b) on the other. For the small capsule, we find  $a_{app}/\ell = 0.85$  or  $a/\ell = 0.86 - 0.87$ ;  $L/\ell = 1.7$ . From figure 12(a,d), we find  $Ca \approx 0.06$  and  $v_o/V = 1.33$ . It follows that

the membrane shear modulus is

$$G_s = \frac{6.6 \times 10^{-3}}{1.33 \times 0.06} = 0.08 \text{ N m}^{-1}. \quad (4.4)$$

The same reasoning for the large capsule yields  $a_{app}/\ell = 1.05$  or  $a/\ell = 1.1 - 1.09$ ;  $L/\ell = 2.5$ ,  $Ca \approx 0.04$  and  $v_o/V = 1.19$ , leading to

$$G_s = \frac{4.5 \times 10^{-3}}{1.19 \times 0.04} = 0.09 \text{ N m}^{-1}. \quad (4.5)$$

These values are in good agreement with those of Lefebvre *et al.* (2008), which is very encouraging. A full analysis of the precision and discriminating power of the method is left for a future study.

## 5. Conclusion

We have shown in this paper how 3D effects affect the flow of capsules in pores with cross-dimensions comparable with the capsule diameter. The confinement effect due to the channel walls compresses the capsule in the direction perpendicular to the pore axis. This leads to compression of the membrane and a tendency towards buckling that has been observed experimentally. The flow of a capsule in a small pore is thus a 3D process even when the pore and the capsule share the same revolution axis.

These 3D effects have been specifically studied and we have shown that in a cylindrical tube with a circular cross-section, the 3D capsule deformation is well approximated by an axisymmetric simple model. This is an interesting and important result as it is much easier and faster to use an axisymmetric numerical model rather than a full 3D model.

In the case of microfluidic pores with square cross-section the 3D aspect of the problem cannot be simplified. We have thus conducted a novel study of the flow of spherical capsules in pores as a function of capillary number and aspect ratio. A comparison between the numerical model and some experimental measurements of capsules flowing in square section microfluidic pores shows that it is possible to evaluate the capsule membrane elastic modulus. This is a very interesting result as it opens the way to the design of on-line microfluidic measuring systems that can evaluate the mechanical properties of capsules.

One of the drawbacks of this study is the lack of bending resistance of the capsule membrane leading to non-physical numerical folds in the regions where the membrane is undergoing compression. Accounting properly for the bending and post-buckling behaviour of the capsule membrane is a formidable problem of shell mechanics. The reason being that the capsule is subjected to large deformation, large membrane forces and that the bending effect becomes preponderant only on parts of the wall. It is clear that a very fine mesh of the capsule wall would be necessary if we were to reproduce the folds with any precision. This would increase very significantly the computer time. The interesting question which arises at this point is how necessary is it to account for bending forces? If the capsule wall has a highly anisotropic structure (e.g. the red blood cell wall which consists of a lipid bilayer lined by a protein network), it is clear that bending forces can be fairly large as compared to membrane shear forces and must be accounted for. For artificial capsules with a wall which consists of a thin layer of a 3D isotropic material (e.g. a gelled membrane reinforced by a polymer network), the bending resistance is directly related to the ratio of the membrane thickness to

the capsule radius. For thickness ratios less than 10%, it is generally admitted that bending effects will be very small compared with the membrane forces. It is thus quite possible that ignoring bending forces and adding a small uncontrolled numerical resistance (due to discretization) leads to a fairly good approximate model that can be used to analyse the motion of real artificial capsules.

### Acknowledgements

This work was supported by the Conseil Régional de Picardie (MODCAP grant), by the French Ministère de la Recherche (Pilcam2 grant) and by the China Scholarship Council (PhD scholarship of X.-Q.H.). The experimental capsule images were graciously provided by Dr E. Leclerc, UMR CNRS 6600, UTC.

### REFERENCES

- BARTHÈS-BIESEL, D. 2011 Modelling the motion of capsules in flow. *Curr. Opin. Colloid Interface Sci.* **16**, 3–12.
- BARTHÈS-BIESEL, D., DIAZ, A. & DHENIN, E. 2002 Effect of constitutive laws for two dimensional membranes on flow-induced capsule deformation. *J. Fluid Mech.* **460**, 211–222.
- CARIN, M., BARTHÈS-BIESEL, D., EDWARDS-LÉVY, F., POSTEL, C. & ANDREI, D. 2003 Compression of biocompatible liquid-filled HSA-alginate capsules: determination of the membrane mechanical properties. *Biotechnol. Bioengng* **82**, 207–212.
- CERDA, E. & MAHADEVAN, L. 2003 Geometry and physics of wrinkling. *Phys. Rev. Lett.* **90** (7), 074302.
- CHU, T. X., SALSAC, A.-V., LECLERC, E., BARTHÈS-BIESEL, D., WURTZ, H. & EDWARDS-LÉVY, F. 2010 Comparison between measurements of elasticity and free amino group content of ovalbumin microcapsule membranes: discrimination of the cross-linking degree. *J. Colloid Interface Sci.* **355**, 81–88.
- COLE, E. T., CAD, D. & BENAMEUR, H. 2008 Challenges and opportunities in the encapsulation of liquid and semi-solid formulations into capsules for oral administration. *Adv. Drug Deliv. Rev.* **60**, 747–756.
- DIAZ, A. & BARTHÈS-BIESEL, D. 2002 Entrance of a bioartificial capsule in a pore. *Comput. Model. Engng Sci.* **3** (3), 321–337.
- DODDI, S. K. & BAGCHI, P. 2008 Lateral migration of a capsule in a plane Poiseuille flow in a channel. *Intl J. Multiphase Flow* **34** (10), 966–986.
- FERY, A. & WEINKAMER, R. 2007 Mechanical properties of micro- and nanocapsules: single capsule measurements. *Polymer* **48**, 7221–7235.
- FINKEN, R. & SEIFERT, U. 2006 Wrinkling of microcapsules in shear flow. *J. Phys.: Condens. Matter* **18** (15), L185–L191.
- GIBBS, B. F., KERMASHA, S., ALLI, I. & MULLIGAN, C. N. 1999 Encapsulation in the food industry: a review. *Intl J. Food Sci. Nutr.* **50**, 213–224.
- HELMY, A. & BARTHÈS-BIESEL, D. 1982 Migration of a spherical capsule freely suspended in an unbounded parabolic flow. *J. Méc. Théor. Appl.* **1** (5), 859–880.
- HUANG, K. S., LIU, M. K., WU, C. H., YEN, Y. T. & LIN, Y. C. 2007 Calcium alginate microcapsule generation on a microfluidic system fabricated using the optical disk process. *J. Micromech. Microengng* **17**, 1428–1434.
- KURIAKOSE, S. & DIMITRAKOPOULOS, P. 2011 Motion of an elastic capsule in a square microfluidic channel. *Phys. Rev. E* **84**, 011906.
- LEFEBVRE, Y. & BARTHÈS-BIESEL, D. 2007 Motion of a capsule in a cylindrical tube: effect of membrane pre-stress. *J. Fluid Mech.* **589**, 157–181.
- LEFEBVRE, Y., LECLERC, E., BARTHÈS-BIESEL, D., WALTER, J. & EDWARDS-LEVY, F. 2008 Flow of artificial microcapsules in microfluidic channels: a method for determining the elastic properties of the membrane. *Phys. Fluids* **20** (12), 123102.

- LUO, H. & POZRIKIDIS, C. 2007 Buckling of a pre-compressed or pre-stretched membrane. *Intl J. Solids Struct.* **44**, 8074–8085.
- MIYAZAWA, K., YAJIMA, I., KANEDA, I. & YANAKI, T. 2000 Preparation of a new soft capsule for cosmetics. *J. Cosmet. Sci.* **51**, 239–252.
- PEDLEY, T. J. 2010 Instability of uniform micro-organism suspensions revisited. *J. Fluid Mech.* **647**, 335–359.
- PEDLEY, T. J. & KESSLER, J. O. 1992 Hydrodynamic phenomena in suspensions of swimming microorganisms. *Annu. Rev. Fluid Mech.* **24**, 313–358.
- POZRIKIDIS, C. 1992 *Boundary Integral and Singularity Methods for Linearized Viscous Flow*. Cambridge University Press.
- POZRIKIDIS, C. 1997 *Introduction to Theoretical and Computational Fluid Dynamics*. Oxford University Press.
- POZRIKIDIS, C. 2005 Numerical simulation of cell motion in tube flow. *Ann. Biomed. Engng* **33**, 165–178.
- QUÉGUINER, C. & BARTHÈS-BIESEL, D. 1997 Axisymmetric motion of capsules through cylindrical channels. *J. Fluid Mech.* **348**, 349–376.
- RABANEL, J. M., BANQUY, X., ZOUAOU, H., MOKHTAR, M. & HILDGEN, P. 2009 Progress technology in microencapsulation methods for cell therapy. *Biotechnol. Prog.* **25**, 946–963.
- RAMANUJAN, S. & POZRIKIDIS, C. 1998 Deformation of liquid capsules enclosed by elastic membranes in simple shear flow: large deformations and the effect of capsule viscosity. *J. Fluid Mech.* **361**, 117–143.
- RISSO, F. & CARIN, M. 2004 Compression of a capsule: mechanical laws of membranes with negligible bending stiffness. *Phys. Rev. E* **69**, 061601–061608.
- RISSO, F., COLLÉ-PAILOT, F. & ZAGZOULE, M. 2006 Experimental investigation of a bioartificial capsule flowing in a narrow tube. *J. Fluid Mech.* **547**, 149–173.
- WALTER, J., SALSAC, A.-V., BARTHÈS-BIESEL, D. & LE TALLEC, P. 2010 Coupling of finite element and boundary integral methods for a capsule in a Stokes flow. *Intl J. Numer. Meth. Engng* **83**, 829–850.
- YEH, C. H., ZHAO, Q., LEE, S. J. & LIN, Y. C. 2009 Using a *t*-junction microfluidic chip for monodisperse calcium alginate microparticles and encapsulation of nanoparticles. *Sensors Actuators* **151**, 231–236.
- ZHANG, H., TUMARKIN, E., PEERANI, R., NIE, Z., SULLAN, R. M. A., WALKER, G. C. & KUMACHEVA, E. 2006 Microfluidic production of biopolymer microcapsules with controlled morphology. *J. Am. Chem. Soc.* **128**, 12205–12210.